

Valley polarization reversal and spin ferromagnetism and antiferromagnetism in quantum dots of the topological insulator monolayer bismuthene on SiC

Mohammadhadi Azari  and George Kirczenow 

Department of Physics, Simon Fraser University, Burnaby, British Columbia, Canada V5A 1S6



(Received 1 July 2019; published 24 October 2019)

The valley and spin polarizations associated with electronic transport in quantum dots of the large-gap topological insulator (TI) monolayer bismuthene on SiC are investigated in the linear response regime using a minimal tight-binding model that accurately describes the low-energy electronic band structure of this TI. It is found that for zigzag edges the electronic edge states are strongly valley polarized if the Fermi energy lies in the bulk energy band gap. We predict the edge-state valley polarizations to switch between valleys K and K' as the Fermi energy varies from the top of the valence band to the bottom of the conduction band or if the direction of electric current through the dot is reversed. If the electrostatic potential in the dot is nonuniform, we predict that the valley polarization of an electron can reverse as it travels through the dot. The valley polarization reversal is due to the zigzag edge-state dispersion crossing the center of the Brillouin zone that separates valleys K and K' and is therefore predicted to be a general phenomenon. Although the spin polarization within the edge states is ferromagnetic, as expected for spin Hall devices, our calculations reveal the out-of-plane component of the spin polarization of the bulk valence band scattering states to be antiferromagnetic, and the direction of the out-of-plane component of the Neel vector to depend on whether the electronic accumulation belongs primarily to valley K or K' .

DOI: [10.1103/PhysRevB.100.165417](https://doi.org/10.1103/PhysRevB.100.165417)

I. INTRODUCTION

Quantum spin Hall (QSH) materials are two-dimensional (2D) topological insulators that support the transmission of electrons through the gapless conducting states at the edges of the system [1–6]. The unique electronic properties of the gapless edge states [5,6], such as their spin polarization [1,2], dissipationless edge currents [1,2], quantized two-terminal conductance $G = 2e^2/h$ [1,2], and robustness against the time-reversal-invariant disorder [1,2], may support future technological applications. One of the serious obstacles to exploiting the potential advantages of the unique properties of the edge states of 2D topological insulators is the small bulk band gap (less than 30 meV) typical of these materials [3,4]. For such small band gaps, thermal excitations of electrons result in competition between edge currents and currents due to the bulk energy bands.

Recently, several theoretical and experimental studies have been carried out on monolayer bismuthene on SiC and have revealed this system to be a promising candidate for a high-temperature 2D topological insulator due to its large (0.86-eV) band gap that arises from the strong spin-orbit coupling of bismuth [7–12]. This work [7–12] has also shown this material to have an indirect bulk band gap. Its conduction band minimum is at the center Γ of the Brillouin zone while the valence band has two maxima (referred to as *valleys*) at the same energy but with differing momenta K and K' [7–12]. Therefore, monolayer bismuthene on SiC is a potential platform for future technologies exploiting the spin and valley degrees of freedom simultaneously. The valleytronic properties of nanostructures of other 2D materials

have attracted much interest. In particular, those of graphene have been studied in depth from a wide variety of perspectives [13–49]. For 2D transition metal dichalcogenides, valleytronics and its interplay with spintronics have been investigated [50–68]. Studies of other 2D systems such as silicene [33,69–81], germanene [33,72,74–81], stanene [33,74,77,78,81–83], SiC nanoribbons [84], and functionalized bismuth [85–88] and antimony [89,90] monolayers have suggested that they should also exhibit pronounced valleytronic effects. However, the valleytronic properties of nanostructures of the topological insulator bismuthene on SiC have not as yet been explored either theoretically or experimentally.

Here, we study the valleytronics of monolayer bismuthene on SiC quantum dots using a minimal tight-binding model developed in Ref. [11]. This model accurately describes the properties of the low-energy band structure of this system including the Rashba valence band splitting and the magnitudes of the direct and indirect band gaps that have been deduced from angle-resolved photoemission and scanning tunneling spectroscopy experiments [8]. This tight-binding model [11] also yields an indirect band gap that is smaller than the direct band gap, as has been predicted by density functional theory based band structure calculations [8].

Calculations of the band structures of 1D zigzag and armchair nanoribbons within this tight-binding model [11] indicate that the model does indeed describe a topological insulator. These band structures (see Fig. 2 of Ref. [11]) exhibit bulk band gaps traversed by gapless edge states as is typical for nanoribbons of 2D topological materials. As has been reported in Ref. [11], these edge states form Kramers pairs related by time reversal and exhibit spin-momentum

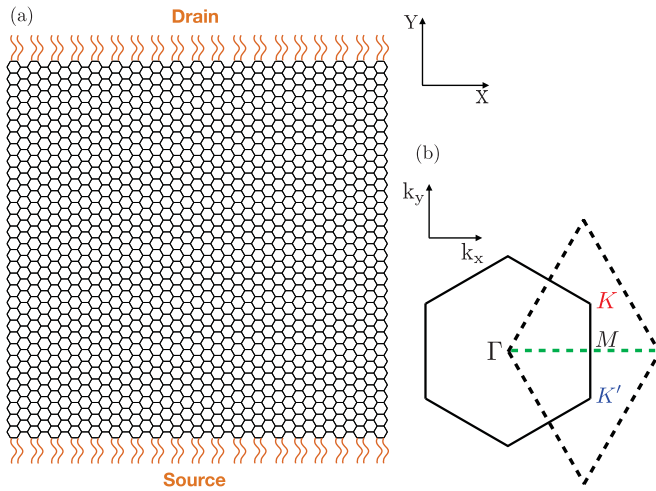


FIG. 1. (a) The bismuthene honeycomb lattice (black) of the two-terminal monolayer bismuthene quantum dot with contacts attached to the armchair edges. Each contact is composed of 38 ideal semi-infinite 1D leads (shown by orange wavy lines). (b) Two alternative representations of the first Brillouin zone of monolayer bismuthene, hexagonal (solid line) and rhombic (dotted line).

locking as is expected for topological insulator edge states. Similar results have also been published by others [8] who also reported calculations of the Z_2 topological invariant that indicate that monolayer bismuthene on SiC is a quantum spin Hall insulator with $Z_2 = 1$.

Within this model, we calculate two-terminal electron Landauer transmission probabilities through quantum dots of bismuthene on SiC, the two contacts each being represented by a group of normal conducting semi-infinite one-dimensional leads; see Fig. 1(a). The scattering states of electrons traveling through the dot at different energies are calculated by solving the Lippmann-Schwinger equation numerically. To investigate the valley polarization of the edge and bulk states of the bismuthene on SiC dot in the linear response regime, these scattering states are projected onto the Bloch states of electrons which are calculated numerically using the tight-binding parameters provided in Ref. [11]. In this way, we generalize to multi-orbital topological insulator nanostructures our previously developed conceptual framework and methodology [37,49] for studying the spatial distribution of the valley polarization in graphene nanostructures.

We find the spatial distribution of the scattering states of the electrons in the quantum dot to take the form of edge states confined near the edges of the system when the Fermi energy lies in the bulk band gap, as is expected for 2D topological insulators. The projection of the scattering states onto the Bloch subspaces of the bismuthene reveals that the conducting channels propagating at zigzag edges of the system are strongly valley polarized if the Fermi level is in the bulk energy band gap. Intriguingly, we also find that the valley polarization of the zigzag edge states switches between valley K and K' as the Fermi energy varies inside the bulk energy band gap. Furthermore, reversing the source and drain contacts (changing the direction of motion of the electrons) also switches the valley polarization of the edge states. It follows that this system offers valley switching mechanisms

(controllable by gating and/or current reversal) that may be exploited in future technologies.

To explore further the reversal of the edge-state valley polarization as the position of Fermi level relative to the band-gap changes, and to study the correlation of the spin and valley degrees of freedom of the electrons of this QSH system, we have modeled an increasing potential energy in the direction parallel to the zigzag edges of the quantum dot. In this model, the dot consists of two regions: Region one, where the Fermi energy lies in the bulk energy band gap, and region two, where the Fermi energy is in the valence band. Although the conduction of the electrons in region one is only mediated by the edge states, in region two both the edge and bulk states conduct the electrons through the quantum dot. We find that, within this model (for fixed Fermi energy), the valley polarization of the same edge state can reverse as the dot is traversed, i.e., the valley polarization of an electron can reverse as it travels through the dot.

We also find the spin polarization in the linear response regime to be ferromagnetic within each edge state but its component perpendicular to the plane of the dot to be antiferromagnetic for the bulk valence band states. In the latter case, the direction of the out-of-plane component of the Neel vector depends on the valley predominantly occupied by the scattering states. To identify the origin of the antiferromagnetic character of the spin polarization of these bulk scattering states and its correlation with the valley polarization, we have calculated the spin polarization of the electrons in an infinite sample of 2D monolayer bismuthene on SiC substrate as a function of the wave vector \mathbf{k} , and found the antiferromagnetism and its correlation with the valley index to be a property of the 2D Bloch states near the valence band maxima.

The remainder of this paper is organized as follows. In Sec. II, the minimal tight-binding model which describes the low-energy band structure of monolayer bismuthene on SiC substrate, the Landauer theory of electron transport, the Lippmann-Schwinger equation, and the method of the projection of the scattering states are explained. We present our results for the valley and spin polarizations calculated for this system in Sec. III. Our conclusions are summarized in Sec. IV.

II. MODEL AND FORMALISM

To describe the quantum dot of monolayer bismuthene on SiC shown in Fig. 1(a), we have used the minimal tight-binding Hamiltonian developed in Ref. [11]. Previous studies have shown that the Bi atoms of monolayer bismuthene on SiC form a planar honeycomb lattice structure with a lattice constant of 5.35 \AA [7,8]. The low-energy band structure of this system is governed by the p_x , p_y , and s valence orbitals of the Bi atoms due to the presence of the SiC substrate which stabilizes the 2D monolayer of Bi atoms and shifts the p_z orbital of the Bi atoms out of the low-energy band structure [8]. The minimal tight-binding Hamiltonian of this system which captures the key qualitative properties of the low-energy band structure and Rashba valence band splitting deduced from the experimental data [8] is of the form [11]

$$H_{i\alpha s, i'\alpha' s'} = H_{\alpha}^0 \delta_{i, i'} \delta_{\alpha, \alpha'} \delta_{s, s'} + H_{i\alpha, i'\alpha'}^{\text{NN}} \delta_{s, s'} + H_{\alpha s, \alpha' s'}^{\text{SO}} \delta_{i, i'} + H_{\alpha s, \alpha' s'}^{\text{R}} \delta_{i, i'}. \quad (1)$$

Here, s and s' are the spin indices, and α and α' denote the $6s$, $6p_x$, and $6p_y$ valence orbitals of the i and i' Bi atoms, respectively. H_α^0 is the energy of valence orbital α , $H_{\alpha\alpha',i\alpha'}^{\text{NN}}$ is the nearest-neighbor hopping energy between the orbital α of atom i and the orbital α' of atom i' , $H_{\alpha s, \alpha' s'}^{\text{SO}}$ is the intra-atomic spin-orbit (SO) interaction, and $H_{\alpha s, \alpha' s'}^{\text{R}}$ describes the atomic Rashba effect which results in the valence band splitting [8,11]. A complete description of this tight-binding Hamiltonian and its parameter values are provided in Ref. [11].

We note that in the present model the tight-binding parameters of the bismuthene edge atoms have been chosen to be the same as those for the bulk. With this choice this model predicts the presence of edge states that have the fundamental properties expected for the edge states of 2D topological insulators for both zigzag and armchair edges, as has been verified in Ref. [11]. Thus, the present model captures the key properties of the edges of 2D topological insulators and allows us to study the properties of topological insulator edge states theoretically. Some indirect experimental evidence for the existence of these edge states for monolayer bismuthene on SiC has been provided by the scanning tunneling spectroscopy experiments reported in Ref. [8]. These experiments found that while there is a large (0.86-eV) gap in the bulk density of states of this material, the density of states at bismuthene edges (that occur at steps in the SiC substrate) is gapless, as is expected if topological insulator edge states are present.

In order to calculate the scattering states involved in electron transmission through the quantum dot at energy E , we have solved the Lippmann-Schwinger equation which is of the form

$$|\psi^l\rangle = |\phi_o^l\rangle + G_o(E)W|\psi^l\rangle, \quad (2)$$

where $|\phi_o^l\rangle$ is an eigenstate of the l th lead that is decoupled from the monolayer bismuthene, $G_o(E)$ is the sum of the Green's functions of the bismuthene quantum dot and the leads at energy E when the leads are decoupled from the dot, W is the coupling between the quantum dot and the leads, and $|\psi^l\rangle$ is the scattering eigenstate of the coupled system if the electron is injected into the quantum dot from the l th lead. The methodology for solving such Lippmann-Schwinger equations is explained in detail in Appendix A of Ref. [37]. The one-dimensional (1D) source and drain leads attached to the topological insulator dot are metallic. The effects of the interfaces between these metallic leads and the topological insulator dot on transport have been studied in depth in Ref. [11]. For the configuration of leads considered in this paper [Fig. 1(a)], it was found in Ref. [11] that the coupling between the leads and edge states of the dot is effectively almost perfect since the calculated conductance of the system of dot plus leads is equal to $2e^2/h$ within machine precision throughout most of the topological insulator bulk band gap, indicating essentially perfect injection of electrons from the source leads into the topological insulator edge states and perfect extraction from the dot edge states into the drain leads.

The next step is the calculation of the valley polarization induced in this QSH system when an electric current passes through it. To this end, we have calculated the Bloch states of electrons in infinite monolayer bismuthene on SiC numeri-

cally, using the tight-binding model Hamiltonian (1) with the parameter values given in Ref. [11]. The Bloch states of the monolayer of Bi atoms in the Dirac notation have the form

$$|\psi_k^j\rangle = \frac{1}{\sqrt{N}} \sum_{i=1}^N e^{i\mathbf{k}\cdot\mathbf{R}_i} \sum_{\alpha=1}^6 \sum_{s=1}^2 C_{i\alpha s}^j(\mathbf{k}) |\alpha_{is}\rangle, \quad (3)$$

where $j = 1, \dots, 12$ stands for the different Bloch states with wave vector \mathbf{k} , i enumerates the unit cells in the monolayer bismuthene, α_{is} denotes the atomic orbitals in unit cell i , \mathbf{R}_i are the Bravais lattice vectors of the monolayer bismuthene. The normalization factor N is chosen to be the total number of the unit cells in the monolayer bismuthene quantum dot. Each Bloch state is assigned to valley K (K') if its wave vector lies within the upper (lower) triangle of the rhombic Brillouin zone separated by the green dotted line shown in Fig. 1(b). Then, the scattering state $|\psi^l\rangle$ for electrons injected into the quantum dot from the l th lead is projected onto the subspaces of the Bloch states of the monolayer bismuthene that belong to valley K and valley K' . Although the Bloch states $|\psi_k^j\rangle$ are defined on a continuum in \mathbf{k} space, in order to evaluate the valley-projected states numerically, we have approximated the continuum by a mesh of \mathbf{k} points. Thus, the projected states are approximated by

$$|\psi_K^l\rangle = B \sum_{j, \mathbf{k} \in K} |\psi_K^j\rangle \langle \psi_K^j | \psi^l \rangle, \quad |\psi_{K'}^l\rangle = B \sum_{j, \mathbf{k} \in K'} |\psi_{K'}^j\rangle \langle \psi_{K'}^j | \psi^l \rangle, \quad (4)$$

where the sums run over the part of the mesh of \mathbf{k} points belonging to valley K or K' and B is the appropriate normalization factor, $B = \frac{\text{number of bismuthene unit cells in the quantum dot}}{\text{total number of } \mathbf{k} \text{ points in the mesh}}$. (Notice that $B = 1$ for the mesh of wave vectors in the Brillouin zone corresponding to waves that obey periodic boundary conditions at the edges of the dot. However, the transport states $|\psi^l\rangle$ do *not* obey periodic boundary conditions. Therefore, a finer mesh is required to project the states $|\psi^l\rangle$ onto the valleys. In this work, the number of mesh points used was sufficient to achieve convergence of the calculated valley polarizations.) Using the calculated projected states, the current-induced average valley accumulation of electrons in valley K (K') at atomic site n , in a two-contact quantum dot (each contact at a specific electrochemical potential μ_i) is defined as [37,49]

$$A_n^{K(K')} = \frac{1}{2\pi} \sum_{l,i} |\langle n | \psi_{K(K')}^l \rangle|^2 \frac{\partial \zeta^l}{\partial E} \Delta \mu_i. \quad (5)$$

In this definition, $\frac{\partial \zeta^l}{\partial E}$ represents the density of states at the Fermi energy in the leads from which electrons flow into the dot and contributes to the dependence of the onsite valley accumulations $A_n^{K(K')}$ on the energy. Here, $|\psi^l\rangle$ originates from the lead l represented by a tight-binding chain so that $\langle n | \psi^l \rangle = e^{i\zeta^l n} + r^l e^{-i\zeta^l n}$, where r^l is the reflection amplitude of $|\psi^l\rangle$ from the nanostructure back into the ideal lead l and E is the energy eigenvalue associated with $|\psi^l\rangle$. We evaluate $A_n^{K(K')}$ in the linear response regime where for the electron source electrode i , $\Delta \mu_i = |eV_{\text{bias}}|$ in Eq. (5) and V_{bias} is the bias voltage applied between the electrodes and is assumed to be small. For the drain $\Delta \mu_i = 0$. Having evaluated the onsite valley accumulations $A_n^{K(K')}$, the onsite valley polarization

of electrons P_n^v in the linear response regime is defined as the difference between the onsite valley accumulations of electrons at atomic site n , so that

$$P_n^v = A_n^K - A_n^{K'}. \quad (6)$$

Consequently, if P_n^v is positive (negative), electrons are predominantly in valley K (K'). Spatial maps of these onsite valley polarizations help to investigate the valley degree of freedom of the edge states in the quantum dot as will be shown in Sec. III.

In order to calculate the onsite spin polarization of the electrons in the monolayer bismuthene on SiC substrate, we have evaluated the expectation value of the spin operator with respect to the scattering states ψ^l at each atomic site. Then, the current-induced onsite spin polarization of the electrons has the form

$$P_{nj}^s = \frac{1}{2\pi} \sum_{l,i} \langle \psi_n^l | S_j | \psi_n^l \rangle \frac{\partial \zeta^l}{\partial E} \Delta \mu_i, \quad (7)$$

where $j = x, y, z$ represents the components of the spin operator \mathbf{S} , and ψ_n^l are the calculated scattering states of electrons at atomic site n . Note that the other terms of this equation are as defined in Eq. (5). We evaluate P_n^s in the linear response regime so that $\Delta \mu_i$ is as defined for Eq. (5) and is assumed to be small.

III. RESULTS

In Figs. 2(a) and 2(b) the calculated onsite valley polarizations P_n^v [Eq. (6)] are represented by red (blue) disks where

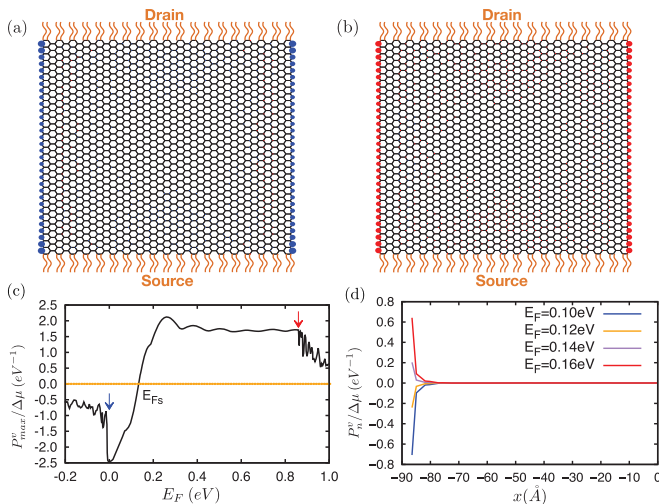


FIG. 2. Spatial maps of the calculated onsite valley polarization P_n^v represented by red (blue) when P_n^v is positive (negative). The diameters of the disks are proportional to the magnitude of the P_n^v . Electron flow is from source (bottom) to drain (top) here and in subsequent figures. Energies are measured from the top of the valence band. (a) $E_F = 0.10$ eV, (b) $E_F = 0.16$ eV. (c) The strongest onsite valley polarization of the zigzag edge states as a function of the Fermi energy. The blue (red) arrow locates the top of the valence band at zero eV (bottom of the conduction band). (d) The onsite valley polarization on a chain of Bi atoms that extends in the x direction from the left zigzag edge to the center of the quantum dot.

they are positive (negative) for Fermi energies in the bulk energy band gap. The diameters of the disks are proportional to the magnitude of the onsite valley polarization P_n^v . Here, the electron flow through the nanostructure is from the source to the drain contact along the zigzag edges of the quantum dot. Since the Fermi energy is inside the bulk band gap, conduction is expected to be localized near the edges of the QSH dot and, therefore, any valley polarization induced by the electric current should also be located close to the dot's edges. Figures 2(a) and 2(b) show that the electric currents do induce valley polarization and that the latter is localized near the zigzag edges of the dot. Representative spatial profiles of the valley polarization are shown in Fig. 2(d). Figure 2(a) (for which the Fermi energy is at 0.10 eV) exhibits valley K' polarization (blue disks) of the edge states, while the valley polarization of the edge states switches to the valley K (red disks) in Fig. 2(b) where the Fermi energy is at 0.16 eV. If we define the valley filter efficiency of the edge states as $\frac{\sum_n A_n^{K(K')}}{\sum_n A_n^K + A_n^{K'}}$, then we find efficiencies of 91.8% and 90.2% in Figs. 2(a) and 2(b), respectively. To gain further insight into this reversal of the valley polarization of the edge states, we have plotted the strongest onsite valley polarization in the quantum dot as a function of the Fermi energy in Fig. 2(c). Figure 2(c) shows that if the Fermi energy is close to the top of valence band (indicated by the blue arrow), the edge states support the transport of electrons accumulating preferentially in valley K' (since P_n^v is negative) and the strength of the valley polarization decreases as the Fermi energy increases. The intersection of the solid black line and the orange dotted line locates the Fermi energy E_{Fs} at which the valley polarization of the edge states switches. When the Fermi energy lies between the E_{Fs} and the bottom of the conduction band (shown by the red arrow), P_n^v is positive and therefore the edge states conduct electrons that accumulate preferentially in valley K . We note also that reversing the source and drain contacts, i.e., changing the direction of motion of electrons (not shown in Fig. 2), also switches the valley polarization of the conducting edge channels. Consequently, the monolayer bismuthene on SiC quantum dot offers practical mechanisms for valley switching based on gate control or reversing the contacts.

The reversal of the valley polarization seen in Fig. 2 as the Fermi energy increases from the top of the bulk valence band to the bottom of the conduction band can be understood as follows: The group velocities of the edge states in Figs. 2(a) and 2(b) both point in the direction from the electron source to the electron drain electrode, i.e., in the positive y direction in Fig. 1. Their magnitudes are both close to 5×10^5 m/s. As can be seen in Fig. 2(a) of Ref. [11], the dispersion of these zigzag edge states is almost linear within the bulk energy gap so that the magnitude of the group velocity is almost independent of the Fermi energy in the gap. More importantly, as the Fermi energy increases from the top of the valence band to the bottom of the conduction band in Fig. 2(a) of Ref. [11], the dispersion $E(k)$ of the edge state with the positive slope (i.e., positive velocity) crosses from left-hand half of the Brillouin zone (where the edge state is in the K' valley) to the right-hand half of the Brillouin zone (where the edge state is in the K valley). This crossing occurs at an energy ~ 0.13 eV

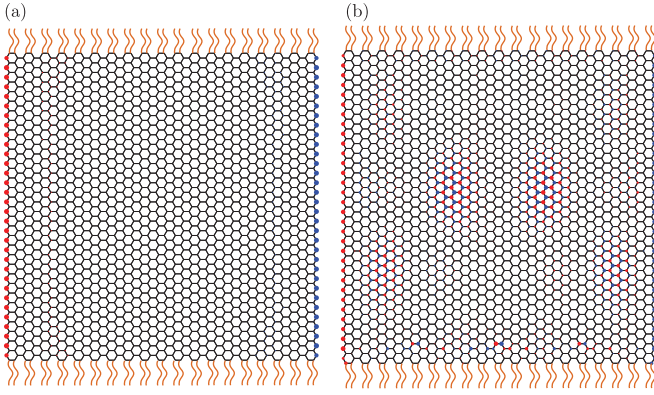


FIG. 3. Spatial map of the calculated onsite out-of-plane component (z direction) of the spin polarization P_{nz}^s represented by red (blue) when P_{nz}^s is positive (negative). (a) Fermi level in bulk band gap $E_F = 0.10$ eV, (b) Fermi level in valence band $E_F = -0.09$ eV.

above the bulk valence band edge. Thus, the reversal of the valley polarization seen at the same energy $E_F \sim 0.13$ eV in Fig. 2(c) is evidently due to the zigzag edge-state dispersion crossing the center of the Brillouin zone from valley K' to valley K at this energy. Consequently, we predict such a reversal of the valley polarization to be a general phenomenon occurring at the zigzag edges of all 2D topological insulators with honeycomb lattices and qualitatively similar edge-state dispersions.

We have also investigated the valley polarization of the armchair edge states of the quantum dot by attaching the leads to the zigzag edges of the quantum dot instead of to the armchair edges as in Fig. 1(a). Our calculations showed that unlike the zigzag edge states, the armchair edge states support no well-defined valley-polarized transport of the electrons in the quantum dot. We interpret this as follows: Comparing Figs. 1(a) and 1(b) it is seen that the vector $\mathbf{K} - \mathbf{K}'$ is perpendicular to armchair edges. Because of this, the armchair edge must cause strong intervalley scattering of electrons so that the armchair edge states are not valley polarized. However, since the zigzag edge is parallel to $\mathbf{K} - \mathbf{K}'$, this argument does not apply to zigzag edges so that zigzag edge states can be valley polarized, consistent with the results presented above.

In order to study possible correlations between the spin and valley polarizations in this QSH system, we have calculated the expectation value of the out-of-plane component of the local spin polarization $\langle S_z \rangle$ when the Fermi energy is inside and outside the bulk energy band gap. Figures 3(a) and 3(b) show the spatial maps of the expectation value of the out-of-plane (z) component of the spin polarization when the Fermi energy is 0.10 eV (in the bulk energy band gap) and -0.09 eV (in the valence band), respectively. The calculated onsite out-of-plane spin polarizations P_{nz}^s are represented by red (blue) disks if they are positive (negative) and the diameter of each disk is proportional to the magnitude of the spin polarization calculated at the corresponding atomic site. As is seen in Fig. 3(a), the edge states located at the opposite edges of the quantum dot have opposite spin polarization. According to Figs. 2 and 3, the degenerate edge states (Kramers pairs)

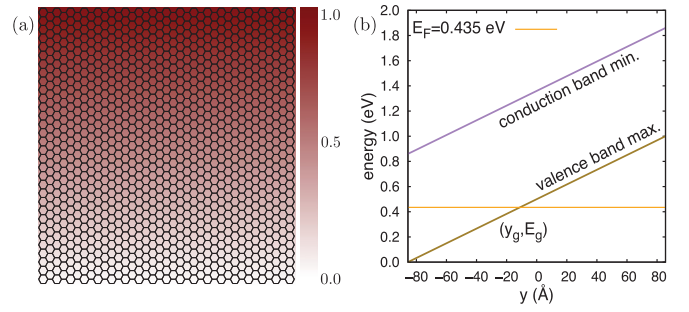


FIG. 4. (a) The profile of the potential energy increasing in the y direction (parallel to the zigzag edge). (b) Schematic representation of the top of valence band (olive green line) and bottom of the conduction band (purple line) when the variable potential energy is included in the model. Energies are measured from the top of the valence band at $y = -85.6$ Å, where $V(y) = 0$. The orange horizontal line locates the Fermi energy for the case considered in Fig. 5.

propagating at opposite edges have the same valley polarization and opposite spin polarization. The latter is characteristic of QSH materials. Since in Fig. 3(b) the Fermi energy is in the valence band, the electron transport is mediated by both the edge and bulk states. While the spin polarization at each edge is ferromagnetic, intriguingly, the spin polarization of the bulk shows antiferromagnetic order in Fig. 3(b). Note that the spin polarization of the zigzag edge states in monolayer bismuthene on SiC is dominated by the out-of-plane component (z direction) while for bulk valence band states this is true only at the valence band maxima.

In Fig. 2(c) a transition is seen from primarily valley K' polarization of the edge states to primarily valley K polarization as the electron Fermi level rises relative to the conduction and valence band edges. This suggests considering also the complementary case in which the energies of the valence and conduction band edges depend on the position in the dot, for instance, due to the presence of multiple gates at suitably chosen applied voltages. In order to investigate this and also the behavior of the out-of-plane component of the spin polarization and the valley polarization when electrons flow from a region where transport is mediated by the edge states (Fermi energy lies in the band gap) to a region where bulk transport is also important (Fermi energy lies in the valence band) we have considered a model in which the electron potential energy depends on the position in the quantum dot as shown in Fig. 4(a). For simplicity we have chosen a linear model potential energy function of the form $V(y) = V_0(y_{\max} + y_n)$, where $V_0 = \frac{1}{171.2}$ eV/Å, $y_{\max} = 85.6$ Å, and y_n is the y coordinate of the n th atomic site, i.e., $V(y)$ increases from 0 for the bottommost atomic sites in Fig. 4(a) to 1 eV for the topmost atomic sites in the y direction, parallel to the zigzag edges of the quantum dot. The effect of the increasing potential energy $V(y)$ on the top of the valence band and bottom of the conduction band as a function of y is represented schematically in Fig. 4(b). In this model, the Fermi energy lies in the bulk energy band gap for the points where it is between the maximum of the valence band and minimum of the conduction band. Consequently, if the

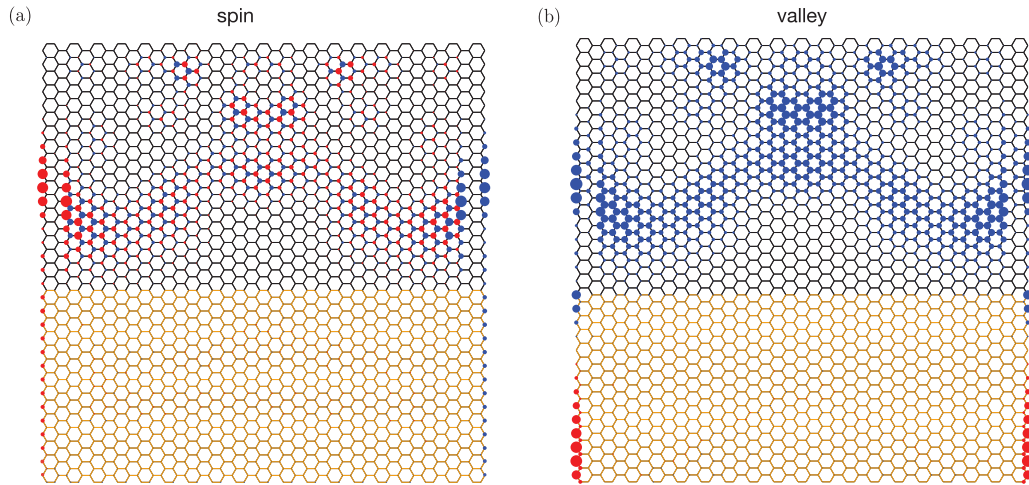


FIG. 5. (a), (b) The spatial map of the out-of-plane component of the spin polarization (S_z) Eq. (7) and onsite valley polarization [Eq. (6)], respectively, when the model potential energy is applied for $E_F = 0.435$ eV. Electron flow is from the bottom to the top of each figure. The meanings of the colors of the red and blue disks are as in Figs. 2 and 3. The region where the Fermi energy lies in (out of) the bulk energy band gap is represented by the orange (black) coloring. Note that the spin and valley polarizations in the orange and black regions are plotted on different scales for clarity. The diameters of the disks plotted in the orange regions representing the spin (valley) polarizations are scaled up by a factor 5 (7) relative to those in the black regions.

Fermi energy coincides with the valence band maximum at $y = y_g$, then in the region of the quantum dot with $y_n < y_g$ only the edge states propagate and in the remaining region we have both bulk and edge states propagating through the nanostructure.

As is seen in Fig. 5(b), the valley polarization of the edge states in the orange region switches from valley K to K' due to the variation of the location of bulk energy band gap relative to the Fermi level as a function of the y coordinate of the atomic sites. Here, for the bottommost atomic sites the Fermi energy E_F is greater than E_{F_s} shown in Fig. 2(c), so the edge states are polarized in valley K . As y_n increases and the top of the valence band approaches E_F ($E_F < E_{F_s}$), the edge states become polarized in valley K' . A comparison of the calculated results of the spin and valley polarization at various Fermi energies shows that increasing the Fermi energy when the potential energy is applied, results in enhancement of y_g shown in Fig. 4(b) and a larger orange region where only the edge states propagate through the system. Interestingly, Fig. 5(b) shows that in the presence of a position-dependent potential, the valley polarization of electrons can reverse when the electrons travel through the quantum dot. It should be noted that the spin and valley polarizations in the orange and black regions of the quantum dot are plotted with different scales for clarity: The diameters of the plotted disks in the orange regions shown in Fig. 5(a) are scaled up by a factor 5 relative to those in the black regions. The corresponding scaling factor is equal to 7 in the case of the valley polarizations plotted in Fig. 5(b).

The out-of-plane spin polarizations shown in Fig. 5(a) reveal that when the Fermi level is in the valence band, the electric current flowing through the dot results in antiferromagnetic order in the interior of the dot, i.e., the expectation values of the z components of the spin angular momenta induced on adjacent bismuth atoms have opposite signs. This

is in contrast to the ferromagnetic order (i.e., parallel spins) within each zigzag edge of the dot that is typical of QSH edge states. We find the antiferromagnetic order seen in the interior of the dot in Fig. 5(a) to be an intrinsic property of the bismuthene valence band Bloch states belonging to the predominantly populated valley. This is demonstrated in Fig. 6(a) which shows the Bloch state expectation values $\langle S_z(k, m) \rangle = \sum_j \langle \psi_k^j(m) | S_z | \psi_k^j(m) \rangle$ of the z components of the spin on the two Bi atoms ($m = 1, 2$) in the unit cell of infinite 2D bismuthene on SiC. Here, k parametrizes the wave vectors along the straight line passing through the valley vectors \mathbf{K} and \mathbf{K}' in the Brillouin zone and the sum is over the two highest (Rashba-split) valence band Bloch states $|\psi_k^j(m)\rangle$ of infinite 2D bismuthene on SiC in the absence of any applied bias. The Bloch states are normalized to 1 in the unit cell. As is seen in Fig. 6(a), the spin expectation values $\langle S_z(k, m) \rangle$ for the two atoms in the unit cell have opposite signs for k in either valley and these signs reverse if k switches to the other valley. The nature of the correlation of the out-of-plane spin and valley polarizations for the valence band Bloch states is also depicted schematically in Fig. 6(b). Namely, if the valence band electrons are polarized in valley K , then the left Bi atom in the unit cell has negative and the right Bi atom has positive out-of-plane spin polarization. However, if the valence band electrons are polarized in valley K' , then the atomic out-of-plane spin polarizations are reversed. These results show that if the Fermi level is in the valence band and there is an imbalance between the populations of the two valleys, then antiferromagnetic order such as that in Fig. 5(a) will be present simply as a consequence of the properties of valence band Bloch states. While in general the Bloch states of infinite 2D monolayer bismuthene on SiC may have nonzero in-plane as well as out-of-plane spin components, we find that the in-plane spin components vanish at the valence band maxima.

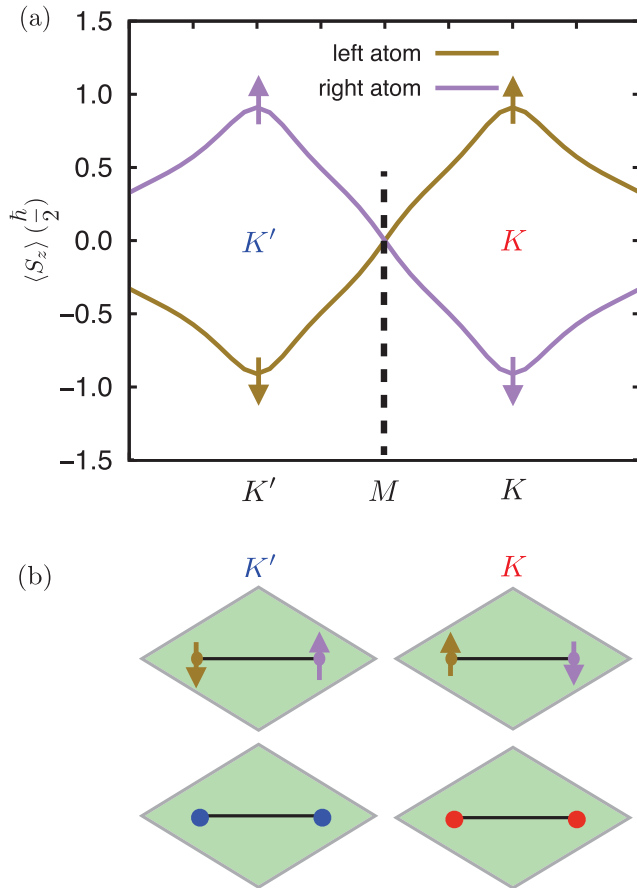


FIG. 6. (a) Expectation values of the out-of-plane component of the spin of electrons occupying valence band Bloch states of the infinite 2D crystal of bismuthene on SiC along a line in k space. K , K' , and M are as in Fig. 1(b). The expectation values are evaluated at the two Bi atomic sites in the crystal unit cell and are summed over the Rashba split valence bands. The black dashed line separates the regions of k belonging to valleys K and K' . (b) Schematic representation of the unit cells of the crystal (green rhombi) showing the out-of-plane atomic spin polarizations from part (a) (olive green and purple arrows shown in the top rhombi) for electrons in valley K and K' . The corresponding valley polarizations at the atoms are indicated by the red and blue disks shown in the bottom rhombi, respectively.

IV. CONCLUSIONS

This paper has investigated the valley and spin polarizations associated with electric currents in quantum dots of monolayer bismuthene on SiC, a potential candidate for a high-temperature topological insulator due to its large bulk energy band gap. The calculated valley polarizations of the edge states in this quantum spin Hall system reveal that the conducting channels localized at the zigzag edges of the quantum dot are strongly valley polarized. The strength and the sign of the valley polarization of these edge states are evaluated as a function of the Fermi energy in the bulk energy band gap. It is shown that the valley polarization of electrons switches between valleys K' and K as the Fermi energy varies from the top of the valence band to bottom of the conduction band in the bulk energy band gap. The calculated results of the spin polarization of the monolayer bismuthene on SiC dot show that the spin polarization of the zigzag edge states is predominantly in the out-of-plane direction. In this quantum spin Hall system, the degenerate edge states propagating at opposite zigzag edges of the system have opposite out-of-plane spin polarizations but the same valley polarization. We have also investigated the out-of-plane spin and valley polarizations of the electrons when the Fermi energy lies outside the bulk energy band gap by considering a position-dependent model potential energy. We predict that if the Fermi energy lies in the valence band, the scattering states propagate through bulk atomic sites of the quantum dots as well as through the edge atomic sites and that the out-of-plane spin polarization of scattering states is antiferromagnetic in the bulk in contrast to the ferromagnetic order at the edges of the system. If the Fermi energy is in the bulk band gap, we find that in the presence of a position-dependent potential it is possible for opposite valley polarizations to be present simultaneously at different positions in the same edge state. Thus, it is possible for the valley polarization of an electron to reverse as it travels through the quantum dot.

ACKNOWLEDGMENTS

This work was supported by NSERC, Westgrid, and Compute Canada.

- [1] C. L. Kane and E. J. Mele, Z_2 Topological Order and the Quantum Spin Hall Effect, *Phys. Rev. Lett.* **95**, 146802 (2005).
- [2] C. L. Kane and E. J. Mele, Quantum Spin Hall Effect in Graphene, *Phys. Rev. Lett.* **95**, 226801 (2005).
- [3] B. A. Bernevig, T. L. Hughes, and S.-C. Zhang, Quantum spin hall effect and topological phase transition in HgTe quantum wells, *Science* **314**, 1757 (2006).
- [4] M. König, S. Wiedmann, C. Brüne, A. Roth, H. Buhmann, L. W. Molenkamp, X. L. Qi, and S. C. Zhang, Quantum spin hall insulator state in HgTe quantum wells, *Science* **318**, 766 (2007).
- [5] M. Z. Hasan and C. L. Kane, Colloquium: Topological insulators, *Rev. Mod. Phys.* **82**, 3045 (2010).
- [6] J. K. Asbóth, L. Oroszlány, and A. Pályi, *A Short Course on Topological Insulators*, Lecture Notes in Physics Vol. 919 (Springer, Berlin, 2016), Sec. 8.4.
- [7] C.-H. Hsu, Z.-Q. Huang, F.-C. Chuang, C.-C. Kuo, Y.-T. Liu, H. Lin, and A. Bansil, The nontrivial electronic structure of Bi/Sb honeycombs on SiC(0001), *New J. Phys.* **17**, 025005 (2015).
- [8] F. Reis, G. Li, L. Dudy, M. Bauernfeind, S. Glass, W. Hanke, R. Thomale, J. Schäfer, and R. Claessen, Bismuthene on a SiC substrate: A candidate for a high-temperature quantum spin Hall material, *Science* **357**, 287 (2017).
- [9] G. Li, W. Hanke, E. M. Hankiewicz, F. Reis, J. Schäfer, R. Claessen, C. Wu, and R. Thomale, Theoretical paradigm for the

- quantum spin Hall effect at high temperatures, *Phys. Rev. B* **98**, 165146 (2018).
- [10] F. Dominguez, B. Scharf, G. Li, J. Schäfer, R. Claessen, W. Hanke, R. Thomale, and E. M. Hankiewicz, Testing topological protection of edge states in hexagonal quantum spin hall candidate materials, *Phys. Rev. B* **98**, 161407(R) (2018).
- [11] G. Kirczenow, Perfect and imperfect conductance quantization and transport resonances of two-dimensional topological-insulator quantum dots with normal conducting leads and contacts, *Phys. Rev. B* **98**, 165430 (2018).
- [12] L. M. Canonico, T. G. Rappoport, and R. B. Muniz, Spin and Charge Transport of Multiorbital Quantum Spin Hall Insulators, *Phys. Rev. Lett.* **122**, 196601 (2019).
- [13] D. Xiao, W. Yao, and Q. Niu, Valley-Contrasting Physics in Graphene: Magnetic Moment and Topological Transport, *Phys. Rev. Lett.* **99**, 236809 (2007).
- [14] A. Rycerz, J. Tworzydło, and C. W. J. Beenakker, Valley filter and valley valve in graphene, *Nat. Phys.* **3**, 172 (2007).
- [15] D. S. L. Abergel and T. Chakraborty, Generation of valley polarized current in bilayer graphene, *Appl. Phys. Lett.* **95**, 062107 (2009).
- [16] T. Nakanishi, M. Koshino, and T. Ando, Transmission through a boundary between monolayer and bilayer graphene, *Phys. Rev. B* **82**, 125428 (2010).
- [17] D. Xiao, M.-C. Chang, and Q. Niu, Berry phase effects on electronic properties, *Rev. Mod. Phys.* **82**, 1959 (2010).
- [18] D. Gunlycke and C. T. White, Graphene Valley Filter Using a line Defect, *Phys. Rev. Lett.* **106**, 136806 (2011).
- [19] L. E. Golub, S. A. Tarasenko, M. V. Entin, and L. I. Magarill, Valley separation in graphene by polarized light, *Phys. Rev. B* **84**, 195408 (2011).
- [20] J.-H. Chen, G. Autès, N. Alem, F. Gargiulo, A. Gautam, M. Linck, C. Kisielowski, O. V. Yazyev, S. G. Louie, and A. Zettl, Controlled growth of a line defect in graphene and implications for gate-tunable valley filtering, *Phys. Rev. B* **89**, 121407(R) (2014).
- [21] R. V. Gorbachev, J. C. W. Song, G. L. Yu, A. V. Kretinin, F. Withers, Y. Cao, A. Mishchenko, I. V. Grigorieva, K. S. Novoselov, L. S. Levitov, and A. K. Geim, Detecting topological currents in graphene superlattices, *Science* **346**, 448 (2014).
- [22] Y. Shimazaki, M. Yamamoto, I. V. Borzenets, K. Watanabe, T. Taniguchi, and S. Tarucha, Generation and detection of pure valley current by electrically induced Berry curvature in bilayer graphene, *Nat. Phys.* **11**, 1032 (2015).
- [23] M. Q. Sui, G. R. Chen, L. G. Ma, W. Y. Shan, D. Tian, K. Watanabe, T. Taniguchi, X. F. Jin, W. Yao, D. Xiao, and Y. B. Zhang, Gate-tunable topological valley transport in bilayer graphene, *Nat. Phys.* **11**, 1027 (2015).
- [24] D. R. da Costa, A. Chaves, S. H. R. Sena, G. A. Farias, and F. M. Peeters, Valley filtering using electrostatic potentials in bilayer graphene, *Phys. Rev. B* **92**, 045417 (2015).
- [25] X. Chen, L. Zhang, and H. Guo, Valley caloritronics and its realization by graphene nanoribbons, *Phys. Rev. B* **92**, 155427 (2015).
- [26] G. Kirczenow, Valley currents and nonlocal resistances of graphene nanostructures with broken inversion symmetry from the perspective of scattering theory, *Phys. Rev. B* **92**, 125425 (2015).
- [27] L. H. Ingaramo and L. E. F. Foa Torres, Valley filtering by a line-defect in graphene: quantum interference and inversion of the filter effect, *J. Phys.: Condens. Matter* **28**, 485302 (2016).
- [28] S.-g. Cheng, J. Zhou, H. Jiang, and Q.-F. Sun, The valley filter efficiency of monolayer graphene and bilayer graphene line defect model, *New J. Phys.* **18**, 103024 (2016).
- [29] A. Cresti, B. K. Nikolić, J. H. Garcia, and S. Roche, Charge, spin and valley Hall effects in disordered graphene, *Riv. Nuovo Cimento* **39**, 587 (2016).
- [30] A. Kundu, H. A. Fertig, and B. Seradjeh, Floquet-Engineered Valleytronics in Dirac Systems, *Phys. Rev. Lett.* **116**, 016802 (2016).
- [31] V. H. Nguyen, S. Dechamps, P. Dollfus, and J.-C. Charlier, Valley Filtering and Electronic Optics Using Polycrystalline Graphene, *Phys. Rev. Lett.* **117**, 247702 (2016).
- [32] M. Settnes, S. R. Power, M. Brandbyge, and A.-P. Jauho, Graphene Nanobubbles as Valley Filters and Beam Splitters, *Phys. Rev. Lett.* **117**, 276801 (2016).
- [33] H. Li, X. Wang, and A. Manchon, Valley-dependent spin-orbit torques in two-dimensional hexagonal crystals, *Phys. Rev. B* **93**, 035417 (2016).
- [34] V. Dal Lago, E. Suárez Morell, and L. E. F. Foa Torres, One-way transport in laser-illuminated bilayer graphene: A Floquet isolator, *Phys. Rev. B* **96**, 235409 (2017).
- [35] J. J. Wang, S. Liu, J. Wang, and F. L. Liu, Valley filter and valve effect by strong electrostatic potentials in graphene, *Sci. Rep.* **7**, 10236 (2017).
- [36] Y. S. Ang, S. A. Yang, C. Zhang, Z. Ma, and L. K. Ang, Valleytronics in merging Dirac cones: All-electric-controlled valley filter, valve, and universal reversible logic gate, *Phys. Rev. B* **96**, 245410 (2017).
- [37] M. Azari and G. Kirczenow, Gate-tunable valley currents, non-local resistances and valley accumulation in bilayer graphene nanostructures, *Phys. Rev. B* **95**, 195424 (2017).
- [38] M. M. Asmar and S. E. Ulloa, Minimal geometry for valley filtering in graphene, *Phys. Rev. B* **96**, 201407(R) (2017).
- [39] D. R. da Costa, A. Chaves, G. A. Farias, and F. M. Peeters, Valley filtering in graphene due to substrate-induced mass potential, *J. Phys.: Condens. Matter* **29**, 215502 (2017).
- [40] T. Sekera, C. Bruder, E. J. Mele, and R. P. Tiwari, Switchable valley filter based on a graphene p-n junction in a magnetic field, *Phys. Rev. B* **95**, 205431 (2017).
- [41] X.-P. Zhang, C. Huang, and M. A. Cazalilla, Valley Hall effect and nonlocal transport in strained graphene, *2D Mater.* **4**, 024007 (2017).
- [42] M. Settnes, J. H. Garcia, and S. Roche, Valley-polarized quantum transport generated by gauge fields in graphene, *2D Mater.* **4**, 031006 (2017).
- [43] T. Farajollahpour and A. Phirouznia, The role of the strain induced population imbalance in valley polarization of graphene: Berry curvature perspective, *Sci. Rep.* **7**, 17878 (2017).
- [44] E. Muñoz and R. Soto-Garrido, Analytic approach to magneto-strain tuning of electronic transport through a graphene nanobubble: Perspectives for a strain sensor, *J. Phys.: Condens. Matter* **29**, 445302 (2017).
- [45] H. Tian and J. Wang, Spatial valley separation in strained graphene pn junction, *J. Phys.: Condens. Matter* **29**, 385401 (2017).

- [46] C. Qu, C. Zhang, and F. Zhang, Valley-selective topologically ordered states in irradiated bilayer graphene, *2D Mater.* **5**, 011005 (2018).
- [47] L. Zhang, Z. Yu, F. Xu, and J. Wang, Influence of dephasing and B/N doping on valley Seebeck effect in zigzag graphene nanoribbons, *Carbon* **126**, 183 (2018).
- [48] C.-S. Park, Valley filtering due to orbital magnetic moment in bilayer graphene, *Phys. Lett. A* **382**, 121 (2018).
- [49] M. Azari and G. Kirczenow, Valley filters, accumulators and switches induced in graphene quantum dots by lines of adsorbed hydrogen atoms, *Phys. Rev. B* **97**, 245404 (2018).
- [50] D. Xiao, G.-B. Liu, W. Feng, X. Xu, and W. Yao, Coupled spin and valley Physics in Monolayers of MoS₂ and Other group-VI Dichalcogenides, *Phys. Rev. Lett.* **108**, 196802 (2012).
- [51] H. Zeng, J. Dai, W. Yao, D. Xiao, and X. Cui, Valley polarization in MoS₂ monolayers by optical pumping, *Nat. Nanotechnol.* **7**, 490 (2012).
- [52] K. F. Mak, K. He, J. Shan, and T. F. Heinz, Control of valley polarization in monolayer MoS₂ by optical helicity, *Nat. Nanotechnol.* **7**, 494 (2012).
- [53] T. Cao, G. Wang, W. Han, H. Ye, C. Zhu, J. Shi, Q. Niu, P. Tan, E. Wang, B. Liu, and J. Feng, Valley-selective circular dichroism of monolayer molybdenum disulphide, *Nat. Commun.* **3**, 887 (2012).
- [54] A. M. Jones, H. Yu, N. J. Ghimire, S. Wu, G. Aivazian, J. S. Ross, B. Zhao, J. Yan, D. G. Mandrus, D. Xiao, W. Yao, and X. Xu, Optical generation of excitonic valley coherence in monolayer WSe₂, *Nat. Nanotechnol.* **8**, 634 (2013).
- [55] K. F. Mak, K. L. McGill, J. Park, and P. L. McEuen, The valley Hall effect in MoS₂ transistors, *Science* **344**, 1489 (2014).
- [56] Y. C. Cheng, Q. Y. Zhang, and U. Schwingenschlöggl, Valley polarization in magnetically doped single-layer transition-metal dichalcogenides, *Phys. Rev. B* **89**, 155429 (2014).
- [57] H. Yu, Y. Wu, G.-B. Liu, X. Xu, and W. Yao, Nonlinear Valley and Spin Currents from Fermi Pocket Anisotropy in 2D Crystals, *Phys. Rev. Lett.* **113**, 156603 (2014).
- [58] A. Srivastava, M. Sidler, A. V. Allain, D. S. Lembke, A. Kis, and A. Imamoglu, Valley Zeeman effect in elementary optical excitations of monolayer WSe₂, *Nat. Phys.* **11**, 141 (2015).
- [59] G. Aivazian, Z. Gong, A. M. Jones, R.-L. Chu, J. Yan, D. G. Mandrus, C. Zhang, D. Cobden, W. Yao, and X. Xu, Magnetic control of valley pseudospin in monolayer WSe₂, *Nat. Phys.* **11**, 148 (2015).
- [60] Y. Li, J. Ludwig, T. Low, A. Chernikov, X. Cui, G. Arefe, Y. D. Kim, A. M. van der Zande, A. Rigosi, H. M. Hill, S. H. Kim, J. Hone, Z. Li, D. Smirnov, and T. F. Heinz, Valley Splitting and Polarization by the Zeeman Effect in Monolayer MoSe₂, *Phys. Rev. Lett.* **113**, 266804 (2014).
- [61] D. MacNeill, C. Heikes, K. F. Mak, Z. Anderson, A. Kormanyos, V. Zolyomi, J. Park, and D. C. Ralph, Breaking of Valley Degeneracy by Magnetic Field in Monolayer MoSe₂, *Phys. Rev. Lett.* **114**, 037401 (2015).
- [62] J. Qi, X. Li, Q. Niu, and J. Feng, Giant and tunable valley degeneracy splitting in MoTe₂, *Phys. Rev. B* **92**, 121403(R) (2015).
- [63] Q. Zhang, S. A. Yang, W. Mi, Y. Cheng, and U. Schwingenschlöggl, Large spin-valley polarization in monolayer MoTe₂ on Top of EuO (111), *Adv. Mater.* **28**, 959 (2016).
- [64] X.-T. An, J. Xiao, M. W.-Y. Tu, H. Yu, V. I. Fal'oko, and W. Yao, Realization of Valley and Spin Pumps by Scattering at Nonmagnetic Disorders, *Phys. Rev. Lett.* **118**, 096602 (2017).
- [65] C. Zhao, T. Norden, P. Zhang, P. Zhao, Y. Cheng, F. Sun, J. P. Parry, P. Taheri, J. Wang, Y. Yang, T. Scrace, K. Kang, S. Yang, G.-x. Miao, R. Sabirianov, G. Kioseoglou, W. Huang, A. Petrou, and H. Zeng, Enhanced valley splitting in monolayer WSe₂ due to magnetic exchange field, *Nat. Nanotechnol.* **12**, 757 (2017).
- [66] N. Singh and U. Schwingenschlöggl, A route to permanent valley polarization in monolayer MoS₂, *Adv. Mater.* **29**, 1600970 (2017).
- [67] X. Chen, L. Zhong, X. Li, and J. Qi, Valley splitting in the transition-metal dichalcogenide monolayer via atom adsorption, *Nanoscale* **9**, 2188 (2017).
- [68] N. Li, J. Zhang, Y. Xue, T. Zhou, and Z. Yang, Large valley polarization in monolayer MoTe₂ on a magnetic substrate, *Phys. Chem. Chem. Phys.* **20**, 3805 (2018).
- [69] M. Ezawa, Spin valleytronics in silicene: Quantum spin Hall-quantum anomalous Hall insulators and single-valley semimetals, *Phys. Rev. B* **87**, 155415 (2013).
- [70] T. Yokoyama, Controllable valley and spin transport in ferromagnetic silicene junctions, *Phys. Rev. B* **87**, 241409(R) (2013).
- [71] M. Tahir and U. Schwingenschlöggl, Valley polarized quantum Hall effect and topological insulator phase transitions in silicene, *Sci. Rep.* **3**, 1075 (2013).
- [72] C. J. Tabert and E. J. Nicol, AC/DC spin and valley Hall effects in silicene and germanene, *Phys. Rev. B* **87**, 235426 (2013).
- [73] Y. Kim, K. Choi, J. Ihm, and H. Jin, Topological domain walls and quantum valley Hall effects in silicene, *Phys. Rev. B* **89**, 085429 (2014).
- [74] M. Ezawa, Monolayer Topological Insulators: Silicene, Germanene, and Stanene, *J. Phys. Soc. Jpn.* **84**, 121003 (2015).
- [75] P. Zhou and L. Z. Sun, 3d Transition Metal Adsorption Induced the valley-polarized Anomalous Hall Effect in Germanene, *Sci. Rep.* **6**, 27830 (2016).
- [76] J. Zhao, H. Liu, Z. Yu, R. Quhe, S. Zhou, Y. Wang, C. C. Liu, H. Zhong, N. Han, J. Lu, Y. Yao, and K. Wu, Rise of silicene: A competitive 2D material, *Prog. Mater. Sci.* **83**, 24 (2016).
- [77] M. Wang, L. Liu, C.-C. Liu, and Y. Yao, van der Waals heterostructures of germanene, stanene, and silicene with hexagonal boron nitride and their topological domain walls, *Phys. Rev. B* **93**, 155412 (2016).
- [78] X. Zhai, S. Wang, and Y. Zhang, Valleyspin Seebeck effect in heavy group-IV monolayers, *New J. Phys.* **19**, 063007 (2017).
- [79] X. Zhai, Y. T. Wang, R. Wen, S. X. Wang, Y. Tian, X. Zhou, W. Chen, and Z. Yang, Valley-locked thermospin effect in silicene and germanene with asymmetric magnetic field induced by ferromagnetic proximity effect, *Phys. Rev. B* **97**, 085410 (2018).
- [80] B. Szafran and D. Zebrowski, Spin and valley control in single and double electrostatic silicene quantum dots, *Phys. Rev. B* **98**, 155305 (2018).
- [81] X. Zhai, J. Gu, R. Wen, R.-W. Liu, M. Zhu, X. Zhou, L.-Y. Gong, and Xing'ao Li, Giant Seebeck magnetoresistance triggered by electric field and assisted by a valley through a ferromagnetic/antiferromagnetic junction in heavy group-IV monolayers, *Phys. Rev. B* **99**, 085421 (2019).

- [82] J. Qi, K. Hu, and X. Li, Electric Control of the Edge Magnetization in Zigzag Stanene Nanoribbons from First Principles, *Phys. Rev. Appl.* **10**, 034048 (2018).
- [83] M. Ghadiyali and S. Chacko, Band splitting in bilayer stanene electronic structure scrutinized via first principle DFT calculations, *Computat. Condens. Matter* **17**, e00341 (2018).
- [84] X. Zheng, X. Chen, L. Zhang, L. Xiao, S. Jia, Z. Zeng, and H. Guo, Perfect spin and valley polarized quantum transport in twisted SiC nanoribbons, *2D Mater.* **4**, 025013 (2017).
- [85] C. C. Liu, J. J. Zhou, and Y. G. Yao, Valley-polarized quantum anomalous Hall phases and tunable topological phase transitions in half-hydrogenated Bi honeycomb monolayers, *Phys. Rev. B* **91**, 165430 (2015).
- [86] W. X. Ji, C. W. Zhang, M. Ding, B. M. Zhang, P. Li, F. Li, M. J. Ren, P. J. Wang, R. W. Zhang, S. J. Hu, and S. S. Yan, Giant gap quantum spin Hall effect and valley-polarized quantum anomalous Hall effect in cyanided bismuth bilayers, *New J. Phys.* **18**, 083002 (2016).
- [87] H. Gao, W. Wu, T. Hu, A. Stroppa, X. R. Wang, B. G. Wang, F. Miao, and W. Ren, Spin valley and giant quantum spin Hall gap of hydrofluorinated bismuth nanosheet, *Sci. Rep.* **8**, 7436 (2018).
- [88] T. Zhou, J. Zhang, H. Jiang, I. Žutić, and Z. Yang, Giant spin-valley polarization and multiple Hall effect in functionalized bismuth monolayers, *npj Quantum Mater.* **3**, 39 (2018).
- [89] T. Zhou, J. Zhang, Y. Xue, B. Zhao, H. Zhang, H. Jiang, and Z. Yang, Quantum spinquantum anomalous Hall effect with tunable edge states in Sb monolayer-based heterostructures, *Phys. Rev. B* **94**, 235449 (2016).
- [90] S. G. Cheng, R. Z. Zhang, J. J. Zhou, H. Jiang, and Q. F. Sun, Perfect valley filter based on a topological phase in a disordered Sb monolayer heterostructure, *Phys. Rev. B* **97**, 085420 (2018).